Nanoemulsions prepared by a two-step low-energy process

Supporting Information

Lijuan Wang[a], Kevin J. Mutch[b], Julian Eastoe[b], Richard K. Heenan[c], Jinfeng Dong[a,*]

[a] *College of Chemistry and Molecular Science, Wuhan University, Wuhan 430072, China*

[b] *School of Chemistry, University of Bristol, Bristol, BS8 1TS, UK*

[c] *ISIS-CCLRC, Rutherford Appleton Laboratory, Chilton, Oxon, OX11 0QX, U.K.*

1. Conductivity measurements in decane/$C_{12}E_5$/water systems

Electrical conductivity is sensitive to the nature and structure of microemulsion systems. Hence, conductivity measurements as a function of water content (10 mM NaCl solution instead as a supporting electrolyte) were performed to determine the microstructure of the concentrates used to make sample A at different water contents. As can be seen in Figure S1, below a weight fraction of water 0.34, the conductivity is very low, consistent with W/O microemulsions (Om) or multiphase systems including liquid crystals (M_{Lc}). As the water content is increased, the conductivity also increases steeply until the water weight fraction, w reaches 0.57. This conductivity behavior may be interpreted as arising from a bicontinuous structure. The conductivity then increases continuously but with a relatively moderate rate beyond this water content. These conductivity data can be used to infer that concentrates with water content in the range of 0.34-0.57 are bicontinuous-type microemulsions.

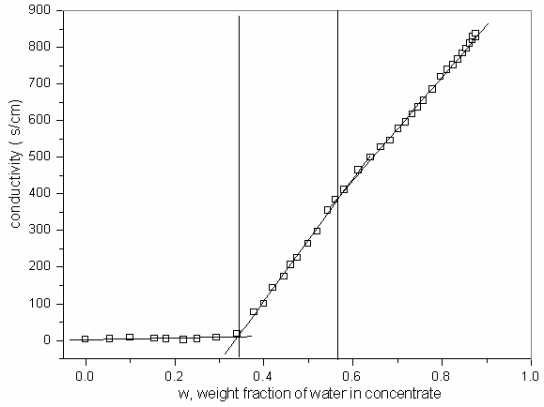

Figure S1. Electrical conductivity as a function of w, the weight fraction of water in the concentrate (sample pathway A).

2. Emulsions prepared by method II in systems with ionic surfactants

Systems with different ionic surfactants, decane/DDAB/water[1], decane/AOT/water (with 100 mM NaCl)[2], dodecane/SDS/pentanol/water[3], and dodecane/CTAB/pentanol/water[3], were formulated to prepare emulsions by the two-step dilution process II (see Experimental section, main paper). The appropriate formulations were chosen as concentrates with reference to literature[1-3], and then injected into water to yield emulsions with a final volume fraction of ϕ=0.030. The equilibrium phase behavior of formulated concentrates and the droplet sizes of resultant emulsions are listed in Table S1. As concentrates formulated with DDAB do not disperse in water at all, there is no DLS data for the droplets obtained in this system.

Table S1. The equilibrium phase behavior of concentrates and the droplet radii of resultant emulsions.

System	w	Temperature (°C)	Equilibrium phase behavior	Droplet radii/nm
Decane/DDAB/water	0.10	25	w/o	-
	0.20	25	Bicontinuous microemulsion	-
	0.80	25	Emulsion	-
Decane/AOT/water (with 100 mM NaCl)	0.10	40	w/o	90
	0.45	40	Bicontinuous microemulsion	60
	0.80	40	Emulsion	293
Dodecane/SDS/pentanol/water	0.10	25	w/o	69
	0.52	25	Bicontinuous microemulsion	83
	0.80	25	Emulsion	222
Dodecane/CTAB/pentanol/water	0.10	25	w/o	65
	0.35	25	Bicontinuous microemulsion	78
	0.80	25	Emulsion	272

Parameter: w is the weight fraction of water in the concentrate.

3. Small-angle neutron scattering

Data were analyzed using standard Guinier limiting laws (see below), and the multi-model FISH fitting program[4], which is based upon an iterative least-squares algorithm. This program allows for various common scattering laws to be tested, the best structural parameters to be obtained and also a measure of the fit residuals (sum of weighed squared errors SWSE). The scattering law used was for Schultz polydisperse spheres[5] with an effective hard-sphere, Percus-Yevick type structure factor S(Q), as solved analytically by Ashcroft and Lekner[6].

The normalised scattered intensity I(Q) is given as:

$$I(Q) = \phi_p \Delta\rho^2 V_p P(Q,R) S(Q) \quad (1)$$

where ϕ_p is the volume fraction of particles; $\Delta\rho = \rho_p - \rho_m$, is the scattering length density difference between particle p and medium m; V_p is the particle volume; P(Q,R) is the single particle form factor arising from intra-particle scattering and S(Q) is the structure factor arising from inter-particle interactions.

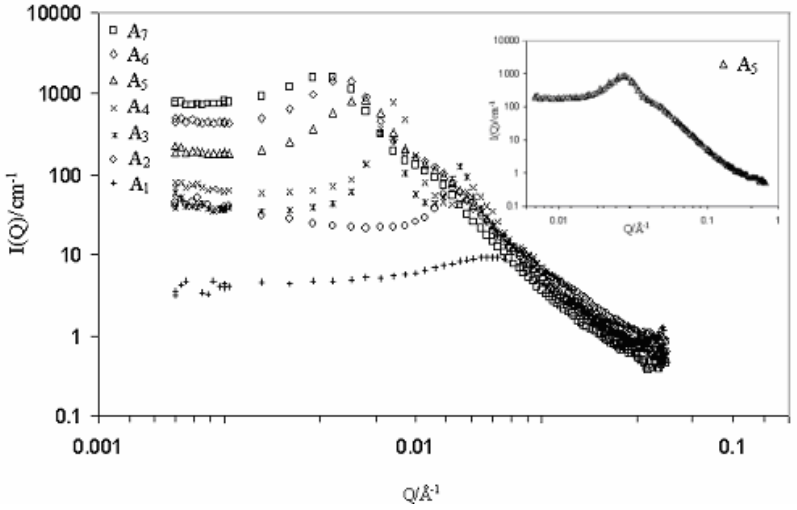

Figure S2. SANS profiles for concentrates A_1-A_7. Inset: shown is the SANS profile of concentrate A_5 separately.

3.1. Guinier limiting laws

The Guinier approximation relates the low Q ($QR_g < 1$) region of the scattering plot to the particle radius of gyration (R_g)[7].

Figure S2 and S3 are Guinier Plots for nanoemulsions at different times and different volume fractions.

Linearity is observed at low Q for spheres (ln I(Q) vs Q^2), and the gradients were used to calculate nanoemulsion radii according to eq. 2. Estimated radii for nanoemulsion at different volume fractions are given in Table 1of the main manuscript and in Table S2 below.

$$\ln[I(Q)] \text{ vs } Q^2: \qquad \text{sphere radius} = \sqrt{\text{slope} \times 5} \tag{2}$$

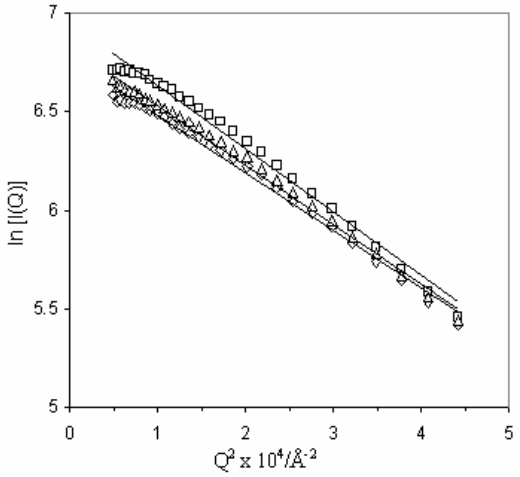

Figure S3. Guinier plot for nanoemulsions (sample pathway A) at different times，t=30(□), 120 (◇) and 240(△).

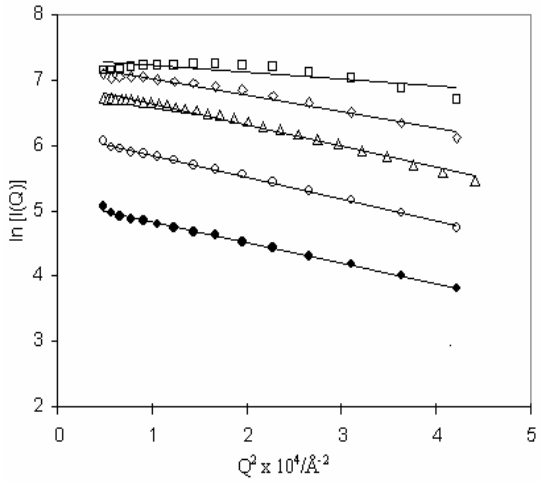

Figure S4. Guinier plot for nanoemulsions with different volume fractions, ϕ=0.120(□), 0.060(◇), 0.030(△), 0.015(○), 0.006(●).

3.2. Porod scattering analysis

At high Q values, the SANS intensity is sensitive to scattering from local interfaces rather than the overall inter-particle correlations. Then I(Q) is related to the total interfacial area S, and the asymptotic intensity may be analysed using the Porod equation[7]:

$$\left\{ \mathrm{I}(Q).Q^4 \right\} = 2\pi\Delta\rho^2\Sigma \tag{3}$$

where Δρ is the contrast step across the interface and Σ is the total interfacial area per unit volume of solution (cm^{-1}). The Porod equation is only valid for smooth interfaces and a Q-range >> 1/R (Porod regime). The droplet radius R may be estimated from the first maximum peak at $Q^1_{max} \approx 2.7/ R$, the first minimum peak at $Q^1_{min} \approx 4.6/ R$, and the second maximum peak at of $Q^2_{max} \approx 6.3/ R$ (Figure S4 and S5)[4]. The three radii obtained are quite close and the deviation is smaller than ±1 nm. The number density of droplets can be obtained by $N_{drop}= \Sigma/4\pi R^2$, where R is the droplet radius. The droplet concentration can then be estimated by $C_{drop}= N_{drop}/N$, where N is the Avogadro's number. The obtained parameters are listed in Table S2. A plot of caluculated droplet concentration against volume fraction shows linearity in

Figure S6.

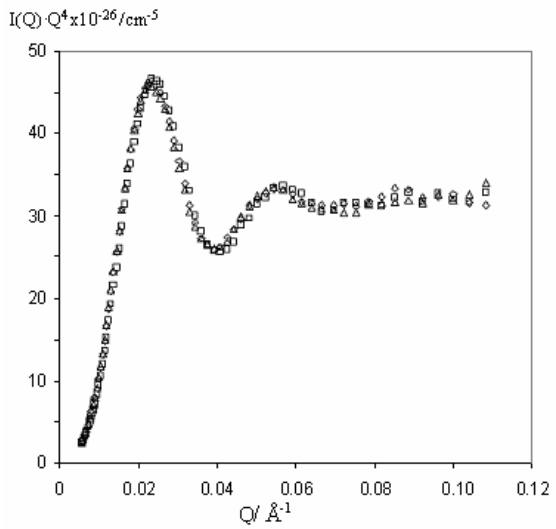

Figure S5. Porod plot for nanoemulsions (pathway A) at different times t=30(▭), 120 (◇) and 240(△).

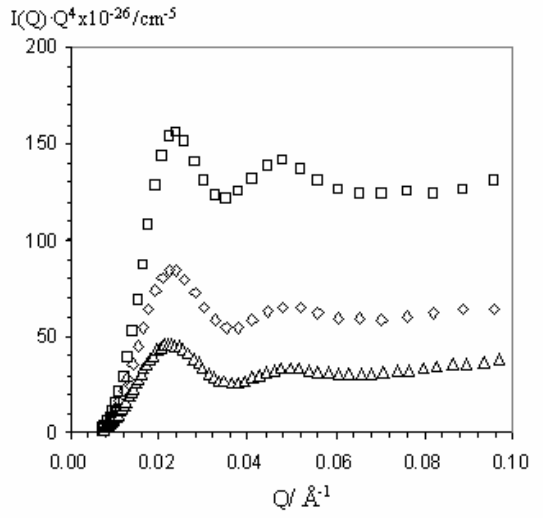

Figure S6. Porod plot for nanoemulsions with different volume fractions, ϕ=0.120(▭), 0.060(◇), 0.030(△).

Table S2. Calculated values estimated by the Guinier and Porod approximation of SANS data[a]

ϕ	Guinier Approximation		Porod Approximation			
	R_g/nm	$R_{Guinier}$/nm	R_{Porod}/nm	Σ/cm^{-1}	N_{drop}/cm^{-3}	C_{drop}/(μmol dm^{-3})
0.120	5.6	7.3	11.3	4.4x10^5	4.2 x10^{16}	69
0.060	8.7	11.2	12.2	2.1 x10^5	1.7 x10^{16}	28
0.030	10.3	13.3	11.9	1.1 x10^5	9.1 x10^{16}	15
0.015	10.1	13.0	11.3	4.2 x10^4	4.0 x10^{15}	7
0.006	9.7	12.5	11.3	1.2 x10^4	1.2 x10^{15}	2

[a] Parameters: R_g and $R_{Guinier}$ are the respective radii of gyration and effecive droplet radius estimated by the Guinier approximation; R_{Porod}, radius estimated by Porod approximation; Σ, the total interfacial area per unit volume of solution; N_{drop}, the number density of droplets; C_{drop}, the calculated nanoemulsion droplet concentration.

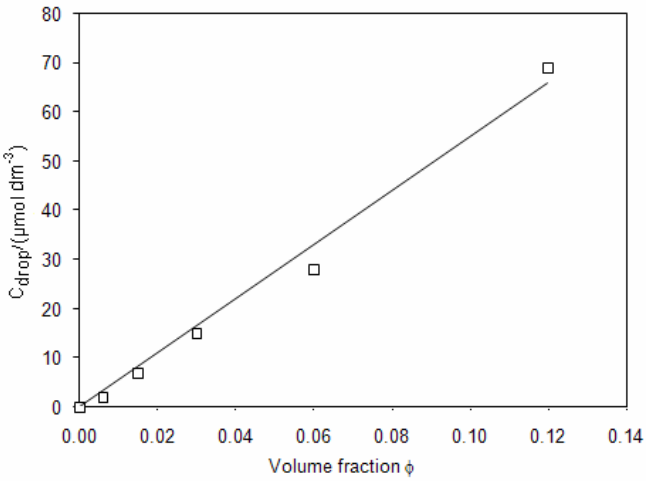

Figure S7. Calculated concentration of droplet against the volume fraction, ϕ

3.3. Schulz polydispersity form factor analyses

The nanoemulsion droplets were treated as spherical particles with a Schultz distribution in radii. Full accounts of the scattering laws are given elsewhere[8-13] and only a summary is necessary here. For polydisperse spherical particles at volume fraction ϕ, radius R_i, volume V_i, and coherent scattering length density ρ_p dispersed in a medium of ρ_m, the normalized SANS intensity $I(Q)$ (cm^{-1}) may be written

$$I(Q) = \phi(\rho_p - \rho_m)^2[\sum_i V_i P(Q,R_i)X(R_i)]S(Q,R_{hs},\phi_{hs}) \quad (4)$$

$P(Q, R_i)$ is the single-particle form factor. The Schultz distribution $X(R_i)$ defines the effective polydispersity using an average radius R^{av} and a root mean squared deviation σ, with z a width parameter. This effective polydispersity function takes into account what are believed to be two dominant contributions to the observed distribution: a natural size polydispersity and thermally excited shape fluctuations. S(Q) is the structure factor, and a hard-sphere model modified for polydispersity was used. This contribution is a function of an effective radius R_{hs} and volume fraction ϕ_{hs}. Since the scattering length densities ρ and volume fractions of the components are all known, three adjustable parameters were required in the analysis: the average micellar radius R_{av}, polydispersity σ/R_{av}, and a scale factor. In the modelling, constraints were $\phi_{hs} = \phi_{oil}+\phi_{surf}$, and $R_{hs} = R_{Porod}^{drop}\pm0.8$ nm. (The subscripts hs, oil and surf denote the hard sphere droplet, oil and surfactant, respectively). For core-shell scattering, the appropriate form factor was used to model the data, as described and employed elsewhere [4, 7, 8.]

Fitted parameters are summarized in Table S3, and the linear relationship between the fitted scale factors can be seen in Figure S7. The inference is that this model gives a reasonable and physically realistic account of the measured scattering curves.

Table S3. Parameters obtained by fitting SANS data to Schultz polydisperse sphere model[a]

ϕ	R_{av}/nm	Fitted scale factor x10^{-4}	σ/R_{av}
0.120	9.4	5.1	0.25
0.060	9.6	2.8	0.26
0.030	10.2	1.6	0.24
0.015	10.3	0.7	0.21
0.006	9.7	0.3	0.20

[a] Parameters: R_{av}, average radius; t_s, apparent shell thickness given by core-shell model; σ/R_c, width of the Schultz distribution function.

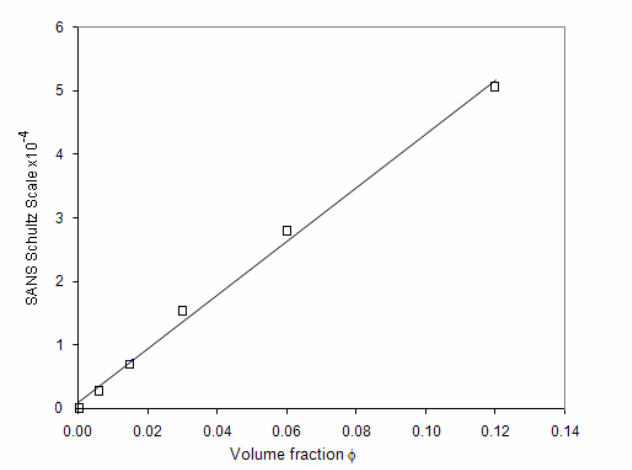

Figure S8. Fitted Schultz scale factors against the nanoemulsion volume fraction, ϕ

4. Stability of nanoemulsions determined by DLS

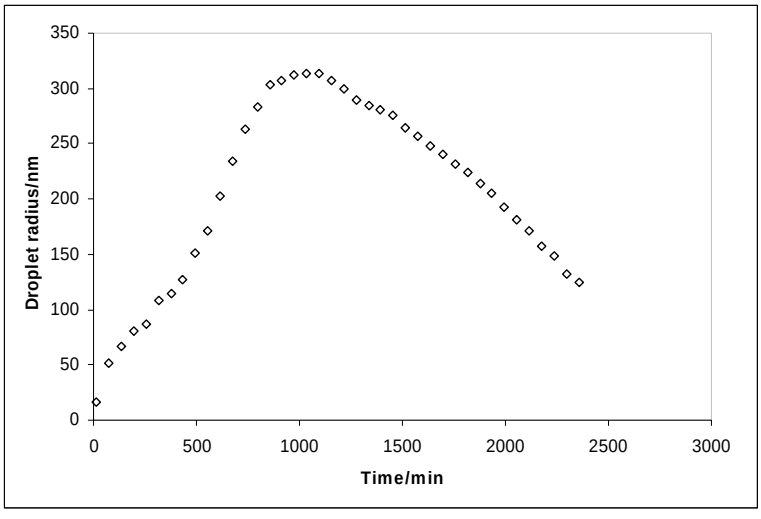

Figure S9. The dependence of apparent droplet radii of nanoemulsion sample A (prepared from A_5) against time at volume fraction ϕ=0.030.

The DLS data were taken from the middle portion of the sample as the apparent droplet sizes evolved. As can be seen from Figure S9, the droplet radii increase with time (1000 min), and then decrease. These

observations are consistent with an initial aggregation (flocculation) of droplets up to ~ 1000 min, and then a slow creaming of larger clusters (flocs), leaving behind a population of smaller flocs as the larger ones cream upwards.

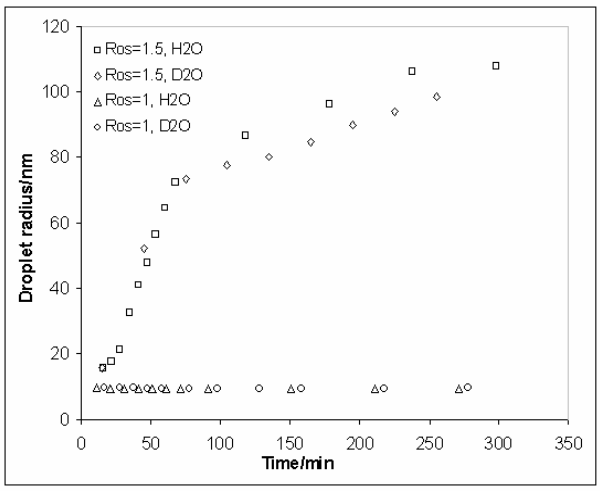

Figure S10. Effect of swapping H_2O for D_2O on the evolution of apparent hydrodynamic radius r_h with time for the microemulsion R_{OS} = 1 and the nanoemulsion sample R_{OS} = 1.5 respectively.

Referecnes

(1) Blum. F.D.; Pickup, S.; Chen, S.J.; Evans, D.F. *J. Phys. Chem.* **1985**, 89, 711-713.

(2) Chen, C.H.; Chang, S.L.; Strey, R.; Samseth, J.; Mortensen, K. *J. Phys. Chem.* **1991**, *95*, 7427-7432

(3) Sripriya, R.; Muthu Raja, K.; Santhosh, G.; Chandrasekaran, M; Noel, M. *J. Colloid Interface Sci.* **2007**, *314*, 712-717.

(4) Heenan, R. K. *Fish Data Analysis Program*, Rutherford Appleton Laboratory, Report RAL-89-129, CCLRC: Didcot, U.K., 1989.

(5) Kotlarchyk, M.; Chen, S-H. *J. Chem. Phys.* **1983**, *79*, 2461-2469.

(6) Ashcroft, N. W.; Lekner, *J. Phys. Rev.* **1966**, *145*, 83-90.

(7) Eastoe, J. Surfactants, Publishers: Wuhan, China, 2005; pp 96-134.

(8) Bumajdad, A.; Eastoe, J.; Nave, S.; Steytler, D. C.; Heenan, R. K.; Grillo, I. *Langmuir* **2003**, *19*, 2560-2567.